DRAFT
CMS Paper

2010/12/24
Head Id: 28691
Archive Id: 28747
Archive Date: 2010/12/23
Archive Tag: trunk

Search for Resonances in the Dilepton Mass Distribution in pp Collisions at $\sqrt{s} = 7$ TeV

The CMS Collaboration

Abstract

A search for a narrow resonance in the dilepton channel has been performed by the CMS Collaboration. The data sample used corresponds to an integrated luminosity of 40 pb^{-1} in the $\mu^+\mu^-$ channel and 35 pb^{-1} in the ee channel, taken in pp collisions at 7 TeV provided by the CERN LHC. Such resonances can arise from heavy gauge bosons Z' or Randall Sundrum Kaluza-Klein gravitons G_{KK}. Upper limits on the inclusive cross section of $Z'/G_{\mathrm{KK}} \to \ell^+\ell^-$ relative to $Z \to \ell^+\ell^-$ are presented. At 95% Confidence Level, the data exclude a Z' with Standard Model-like couplings below 1140 GeV, the superstring-inspired Z'_ψ below 887 GeV, and Kaluza-Klein gravitons below 855-1079 GeV for couplings of 0.05-0.1.

1 Introduction

Many models of new physics predict the existence of a narrow resonance, possibly at the TeV mass scale, that decays to a pair of charged leptons. This paper describes a search for resonant signals that can be detected by the Compact Muon Solenoid (CMS) detector at the Large Hadron Collider (LHC) [1] at CERN. These could arise from additional heavy neutral gauge bosons Z' (spin 1), predicted by grand unified theories [2], as well as Kaluza-Klein (KK) graviton excitations G_{KK} (spin 2) arising in the Randall-Sundrum (RS) model of extra dimensions [3, 4]. For a resonance mass of 1 TeV, the widths are 30, 6, 14 and 3.5 GeV for a Z'_{SSM}, Z'_{ψ}, and G_{KK} with coupling $k/\overline{M_{Pl}}$ =0.05 and 0.1, respectively. Narrow $Z' \rightarrow \ell^+\ell^-$ and $G_{KK} \rightarrow \ell^+\ell^-$ resonances have previously been searched for in $p\bar{p}$ collisions at the Tevatron [5–8] with over 4 fb^{-1} of integrated luminosity at center-of-mass energy of 1.96 TeV. By examining the cross sections and angular distribution of dileptons and other hadronic final states in e^+e^- collisions, indirect constraints on the mass of the virtual Z' bosons have been placed by LEP-II experiments. [9].

The results presented in this paper are obtained from an analysis of the 2010 data set corresponding to an integrated luminosity of 40 pb^{-1} in the $\mu^+\mu^-$ channel, and 35 pb^{-1} in the ee channel, obtained with pp collisions at a center-of-mass energy of 7 TeV. By examining the dilepton mass spectrum from below the Z pole to the highest-mass events recorded, we obtain in a robust manner (weakly dependent on parton distribution functions) the ratio of the production cross section times branching fraction for high-mass resonances to that of the Z. This search for resonances is based on a shape analysis in order to be robust against uncertainties in the absolute background level. Using further input describing the dilepton mass dependence of effects of parton distribution functions and K-factors, mass bounds are calculated on specific models, as well as model independent limit contours and lower bounds on selected benchmark models for Z' production in the two-parameter (c_d, c_u) plane [10].

The central feature of the Compact Muon Solenoid (CMS) [11] apparatus is a superconducting solenoid, of 6 m internal diameter, providing a field of 3.8 T. Within the field volume are the silicon pixel and strip trackers, the crystal electromagnetic calorimeter (ECAL) and the brass/scintillator hadron calorimeter (HCAL). Muons are measured in gas-ionization detectors embedded in the steel return yoke. In addition to the barrel and endcap detectors, CMS has extensive forward calorimetry.

For the data sample presented in this paper, the performance of the detector systems is established using measurements of standard model (SM) W and Z processes with leptonic final states [12]. Muons are measured in the pseudorapidity range $|\eta| < 2.4$, with detection planes made of three technologies: drift tubes in the barrel region, cathode strip chambers in the endcaps, and resistive plate chambers in the barrel and part of the endcap. The inner tracker (silicon pixels and strips) detects charged particles within the pseudorapidity range $|\eta| < 2.5$. It provides an impact parameter resolution of $\sim$ 15 μm and a transverse momentum (p_T) resolution of about 4 % for 500 GeV particles. The electromagnetic calorimeter provides coverage in pseudorapidity $|\eta| < 1.479$ in a cylindrical barrel region (EB) and $1.479 < |\eta| < 3.0$ in two endcap regions (EE). A preshower detector consisting of two planes of silicon sensors interleaved with a total of 3 X_0 of lead is located in front of the EE.

The first level (L1) of the CMS trigger system, composed of custom hardware processors, selects the most interesting events using information from the calorimeters and muon detectors. The High Level Trigger (HLT) processor farm further decreases the event rate with access to the full event information including the inner tracker. The muon paths of the HLT use information from the muon detectors and the silicon pixel and strip trackers. The electromagnetic trigger paths of the HLT use the energy deposits in the ECAL and HCAL and the electron triggers in addition require tracks matched to clusters. Events with muons or electromagnetic clusters with p_T above L1 and HLT thresholds are recorded.

2 Electron and Muon Selection

2.1 Triggers

The events used in the dimuon channel analysis were collected using a single muon trigger that required $p_T > 9$, 11 or 15 GeV, depending on the running period. A double electromagnetic (EM) cluster trigger was used to select the events for the dielectron channel. ECAL clusters are formed by collecting energy deposits in crystals surrounding a 'seed' that is locally the highest-energy crystal. This trigger requires two clusters in the ECAL with an energy transverse to the beam direction E_T above a threshold of 17-22 GeV, depending on the running period. For each of these clusters, the ratio of the energy of the HCAL cells situated behind the ECAL cluster to the ECAL cluster's energy (H/E), is required not to exceed 15%. One of these clusters must have been found by the L1 trigger.

2.2 Lepton reconstruction

The reconstruction, identification, and calibration of electrons [12] and muons [13] follow standard CMS methods.

Muons are reconstructed as tracks both in the muon detectors and the silicon tracker. The two can be matched and fitted simultaneously to form a "global muon". Both muons in the event must be identified as global muons with at least 10 hits in the silicon tracker and each have $p_T > 20$ GeV. All muon candidates that satisfy these criteria are classified as "loose" muons. At least one of the two muons in each event must be further classified as "tight" muon by passing the following additional requirements: a transverse impact parameter with respect to the collision point less than 0.2 cm; a χ^2 per degree of freedom less than 10 from the global track fit; at least one hit in the pixel detector; hits from the muon tracking system in at least two muon stations on the track; and the muon must have been found by the single muon trigger.

Electrons are reconstructed by associating a cluster in the ECAL with a track in the tracker. Track reconstruction, which is specific to electrons to allow for bremsstrahlung emission, is seeded from the clusters in the ECAL, first using the cluster position and energy to search for compatible hits in the pixel detector, and then using these hits as seeds to reconstruct a track in the silicon tracker. A minimum of five hits is required on each track. Electron candidates must fall within the barrel or endcap acceptance regions, with pseudorapidities of $|\eta| < 1.442$ and $1.560 < |\eta| < 2.5$, respectively. A candidate electron is required to deposit most of its energy in the ECAL and relatively little in the HCAL ($H/E < 5\%$). The transverse shape of the energy deposit is required to be consistent with that expected of an electron, and the associated track must be well-matched in η and ϕ. Electron candidates must have an $E_T > 25$ GeV.

In order to suppress fake leptons from jets and non-prompt muons from hadron decays both lepton selections impose isolation requirements. Candidate leptons are required to be isolated within a narrow cone of radius $\Delta R = \sqrt{(\Delta\eta)^2 + (\Delta\phi)^2} = 0.3$, centered on the lepton. Muon isolation requires that the sum of the p_T of all tracks (excluding the muon) is less than 10% of the p_T of the muon. For electrons the sum of the p_T of the tracks excluding the tracks within an inner cone of 0.04 is required to be less than 7 GeV for candidates reconstructed within the barrel acceptance and 15 GeV within the endcap acceptance. The calorimeter isolation requirement for candidates within the barrel acceptance is that, excluding the candidate E_T the sum of the E_T resulting from deposits in the ECAL and the HCAL within a cone of 0.3 is less than $0.03E_T$ + 2 GeV. For candidates within the endcap acceptance the radial segmentation of the HCAL is exploited. For candidate E_Ts less than 50 GeV (above 50 GeV) the isolation energy is required to be less than 2.5 GeV ($0.03(E_T - 50) + 2.5GeV$), where this E_T is determined using the ECAL and first segmented layer of the HCAL. The E_T in the second layer of the HCAL is required to be less than 0.5 GeV. These requirements ensure that the candidate electrons are well-measured and have minimal contamination from jets.

A combination of test beam, cosmic muons and data from proton collisions have been used to calibrate the relevant detector systems for both muons and electrons.

The muon system momentum resolution varies from 1% at energies of a few tens of GeV to 10% at energies of several hundred GeV, consistent with measurements made with cosmic rays [14]. Alignment of the muon and inner tracking systems is important for the obtaining the best resolution for momentum, and thus for mass, particularly at the high masses relevant to the Z′ search. An additional contribution to the momentum resolution arises from the presence of distortion modes in the tracker that are not completely constrained by the alignment procedures. The mass resolution is estimated to have an rms resolution of 5.8% at 500 GeV and 9.6% at 1 TeV.

The ECAL has an ultimate energy resolution of better than 0.5% for unconverted photons with transverse energies above 100 GeV. The ECAL energy resolution obtained thus far is on average 1.0% for the barrel and 4.0% for the endcaps. This calibration was validated by electrons from W and Z bosons. For both muons and electrons, the energy scale is set using the Z mass peak except for electrons in the barrel section of the ECAL, where the energy scale is fixed using neutral pions. The energy scale uncertainty is 1% in the barrel and 3% in the endcaps.

2.3 Efficiency estimation

The efficiency for identifying and reconstructing lepton candidates is measured with the 'tag-and-probe' method [12]. A tag lepton is established by applying tight cuts to one lepton candidate; the other candidate is used as a probe. A large sample of high-purity probes is obtained by requiring that the tag-and-probe pair have an invariant mass compatible with the Z boson mass ($80 < m_{\ell\ell} < 100$ GeV). Several factors contributing to the overall efficiency are measured, including the trigger efficiency, silicon track reconstruction efficiency, electron clustering efficiency and the lepton reconstruction and identification efficiency. All efficiencies and scale factors quoted below are computed using events in the Z mass region.

The trigger efficiencies are defined relative to the full offline lepton requirements. For di-electron events, the double EM cluster trigger is 100% efficient (99% during the early running period). For the dimuon events, the efficiency of the single muon trigger with respect to loose muons is measured to be 89% $\pm$ 2% [12]. The total efficiency for loose (tight) muons is measured to be 94.1% $\pm$ 1.0% (81.2% $\pm$ 1.0%). Within the statistical precision limited by the current data sample, the efficiency value is constant as a function of p_T above 20 GeV as is the ratio to the Monte Carlo (MC) prediction. For electrons, the total efficiency is 90.1% $\pm$ 0.5% (barrel) and 87.2% $\pm$ 0.9% (endcap). The ratio of the electron efficiency measured from the data to that determined from MC simulation at the Z pole is found to be 0.979 $\pm$ 0.006 (barrel) and 0.993 $\pm$ 0.011 (endcap). To determine the efficiency applicable to high energy electrons in the data sample, this correction factor is applied to the efficiency found using MC simulation. From MC simulation, the efficiency of electron identification is found to increase as a function of the electron transverse energy until it becomes flat beyond an E_T value of about 45 GeV.

Simulated event samples for the signal and associated backgrounds were generated with the PYTHIA [15] MC event generator, and with MADGRAPH [16] and POWHEG [17–19] interfaced with the PYTHIA parton-shower generator. The response of the detector was simulated in detail using GEANT4 [20]. These samples were further processed through the trigger emulation and event reconstruction chain of the CMS experiment.

A data set corresponding to 40 pb^{-1} of accumulated luminosity is used for the dimuon analysis. The dielectron sample corresponds to an integrated luminosity of 35 pb^{-1}. The electron event sample is smaller because of tighter data quality requirements imposed on data collected by the calorimeters.

For both final states, two same flavour leptons are required that pass the lepton identification criteria in section 2.2. The two charges are required to be opposite sign in the case of dimuons (for which a charge mis-assignment implies a large momentum measurement error), but not in the case of dielectrons (for which charge mis-assignment is decoupled from the ECAL-based energy measurement). An opposite-charge requirement for dielectrons would lead to non-negligible loss of signal efficiency.

Electrons and muons are required to have $E_T > 25$ GeV and $p_\mathrm{T} > 20$ GeV, respectively. The electron sample requires at least one electron candidate in the barrel since events with both in the endcaps will have a lower signal-to-background ratio. Two isolated loose muons are selected, with one of them required to satisfy the "tight" criteria. For both channels, each event is required to have a reconstructed vertex with at least four associated tracks, located less than 2 cm from the center of the detector in the direction transverse to the beam and less than 24 cm in the direction along the beam. This requirement provides protection against any anomalous conditions in beam bunch crossings and cosmic rays.

All acceptances for the Z' signal as a function of mass are found using MC simulation. The efficiencies for identifying muons or electrons are determined from data in the Z mass region, as outlined earlier. The ratio of efficiency$\times$acceptance for lepton pairs from Z' compared to that from the Z bosons varies with invariant mass from 1.5 (2.0) for muons at 200 (1000) GeV and 1.7 (2.4) for electrons at 200 (1000) GeV. Uncertainties of 3% and 8% are assigned to these values for the dimuon and dielectron samples respectively. These arise from the mass dependence of the acceptance ratio and selection efficiencies of the events in the high mass region compared to those in the Z mass region.

3 SM Backgrounds

The most prominent SM process which contributes to the $\mu^+\mu^-$ and e^+e^- invariant mass spectra is the Drell-Yan process (Z/γ^*), with additional contributions from the $t\bar{t}$, tW, WW, and $Z \to \tau\tau$ processes. In addition, jets may be misidentified as leptons, and contribute to the dilepton invariant mass spectrum through multi-jet and vector boson + jet processes.

3.1 Z/γ^* Backgrounds

The shape of the dilepton invariant mass spectrum is predicted from Drell-Yan production using a MC simulation based on the PYTHIA event generator. While the search for resonances only uses the shape for the comparisons with expectations, the simulated spectrum at the invariant mass peak of the Z boson is normalized to the data. For the dielectron analysis, the data events in the Z mass region between $80-100$ GeV are used, while the dimuon analysis is normalized using data events in the invariant mass region between $60-120$ GeV. A component of the uncertainty in extrapolating the event yield and the shape of the Drell-Yan background to high invariant masses arises from higher order QCD corrections. The next-to-next-to leading order (NNLO) K-factor is computed using FEWZz [21] with PYTHIA and CTEQ6.1 as a baseline, and it is found that the variation of the K-factor with mass does not exceed 8%, where the main difference arises from the comparison of PYTHIA and FEWZz calculations. A further source of uncertainty arises from the parton distribution functions (PDF). The LHAGLUE [22] interface to the LHAPDF [23] library is used to evaluate these uncertainties, using the error PDFs from the CTEQ6.1 and the MRST2006nnlo PDF sets. The resulting uncertainty in the number of events normalized to those expected at the Z peak is about 4% for $\ell\ell$ masses between 200 GeV and 1 TeV.

3.2 Other Backgrounds with Prompt Lepton Pairs

The dominant non-Drell-Yan electroweak contribution to the tail of the $m_{\ell\ell}$ distribution is $t\bar{t}$, with additional contributions from tW and diboson production. In the Z peak region, $Z \to \tau\tau$ decays also contribute. All these processes are flavour-symmetric and so have branching ratios to a pair of leptons of different flavour, $e\mu$, which are twice the size of those to ee or $\mu\mu$ alone. The invariant mass spectrum from $e^{\pm}\mu^{\mp}$ events should have the same shape as that of same flavour $\ell^+\ell^-$ events but without significant contamination from Drell-Yan production.

Figure 1 shows the observed $e^{\pm}\mu^{\mp}$ dilepton invariant mass spectrum from a dataset corresponding to 35 pb^{-1}, overlaid on the prediction from simulated background processes. This spectrum was acquired using the same single muon trigger as in the dimuon analysis and by requiring oppositely charged leptons. Using an electron trigger, a very similar spectrum is produced. Differences in the acceptances and efficiencies result in the predicted ratios of $\mu^+\mu^-$ and ee to $e^{\pm}\mu^{\mp}$ being approximately 0.64 and 0.50, respectively. In the data, shown in figure 1, there are 31 (7) $e^{\pm}\mu^{\mp}$ events with invariant mass above 120 (200) GeV. This yields an expectation of about 20 (5) $\mu^+\mu^-$ events and 16 (3) ee events. A direct estimate from Monte Carlo simulations of the processes involved predicts $20.1 \pm 3.6 (5.3 \pm 0.96)$ $\mu^+\mu^-$ events, and 12.5 ± 2.9 (3.3 ± 0.8) ee events. The uncertainty includes both statistical and systematic sources, and is dominated by the theoretical uncertainty on the $t\bar{t}$ production cross section [24] of 15%. The good agreement between the observed and predicted distributions provides a validation of the contributions from the backgrounds from prompt leptons estimated using MC simulations.

3.3 Events with Misidentified and Non-Prompt Leptons

A further source of background arises where objects are falsely identified as prompt leptons. The principal source is jets misidentified as leptons, more likely to occur for electrons than for muons.

Backgrounds arising from jets that are misidentified as electrons include $W \to e\nu$ + jet events with one jet misidentified as a prompt electron, as well as multi-jet events with two jets faking prompt electrons. A prescaled single EM cluster trigger is used for collecting a sample of events to determine the rate of jets misreconstructed as electrons and to estimate the backgrounds from misidentified electrons. The probability of a EM cluster with $H/E < 5\%$ to be reconstructed as an electron is determined from a data sample dominated by multi-jet events. The events in this sample are required to have no more than one reconstructed electron, and missing transverse energy of less than 20 GeV to suppress the contribution from Z and W events, respectively. The probability of a EM cluster with $H/E < 5\%$ to be reconstructed as an electron is determined in bins of E_T and η, and is used to appropriately weight events which have two such clusters passing the double EM trigger. This provides an estimate of the contribution to the dielectron

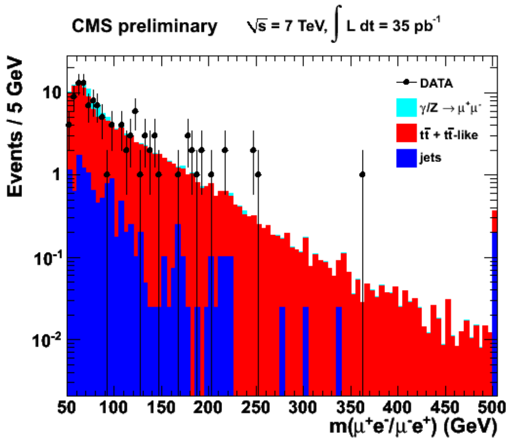

Figure 1: The observed opposite-sign $e^{\pm}\mu^{\mp}$ dilepton invariant mass spectrum (data points). The solid histogram shows the contribution to the spectrum from Z/γ^*, $t\bar{t}$, $t\bar{t}$-like (tW, diboson production $Z \rightarrow \tau\tau$), and the multi-jet background (the latter taken from Monte Carlo simulation).

mass spectrum from jet events giving 8.6±3.4 (2.1±0.8) background events from this source for $m_{ee} > 120$ (200) GeV.

In order to estimate the residual contribution from background events with at least one non-prompt or misidentified muon, events are selected from the data sample with single muons that pass all selection cuts except the isolation requirement. A map of the probability that these muons are isolated as a function of p_{T} and η is created. This probability map is corrected for the expected contribution from events with single prompt muons from $t\bar{t}$ and W decays and for the observed correlation between the probabilities for two muons in the same event. This probability map is used to predict the number of background events with two isolated muons based on the sample of events that have two non-isolated muons. This procedure has been validated using simulated events. From the data, on average there should be 0.8 ± 0.2 (0.20 ± 0.08) background events from this source for $m_{\mu\mu} > 120$ (200) GeV.

As the signal sample includes the requirement that the muons in the pair have opposite electric charge, a further cross-check of this estimate is performed using events with two isolated muons of the same charge. Background events with non-prompt muons should contain muon pairs with same and opposite charge with equal probability. There are no events with same-charge muon pairs and $m_{\mu\mu} > 120$ GeV, which is statistically compatible with the 1.5 ± 0.3 events from SM processes predicted using the MC simulation.

3.4 Cosmic-Ray Muon Backgrounds

The $\mu^+\mu^-$ data sample is susceptible to contamination from cosmic-ray muons, which can be reconstructed as a pair of oppositely-charged, high-momentum muons. Cosmic-ray events can be removed from the data sample because of their distinct topology (collinearity of two tracks originating from the same muon), and since they do not originate from the collision point their impact parameters with respect to the collision vertex are uniformly distributed. Based on these properties, these events are removed from the data sample. A suppression of cosmic-ray muons is obtained by requiring that the three-dimensional angle between the two muons to be greater than 0.02 rad. The residual mean expected background is measured to be less than 0.1 events from cosmic-ray muons with an invariant mass above 120 GeV.

4 Dilepton Invariant Mass Spectra

The measured $\mu^+\mu^-$ and ee invariant mass spectra are displayed in Fig. 2(a) and (b) respectively, along with the expected signal from Z'_{SSM} with a mass of 750 GeV. In the dimuon sample, the highest invariant mass event has $m_{\mu\mu} = 463$ GeV, with the p_T of the two muons measured to be 258 and 185 GeV. The highest invariant mass event in the dielectron sample has $m_{ee} = 419$ GeV, with the electron candidates having E_T of 125 and 84 GeV.

The expectations from the various background sources, Z/γ^*, $t\bar{t}$, $t\bar{t}$-like (tW, diboson production, $Z \rightarrow \tau\tau$) and non-prompt or misidentified muons are also overlaid in Fig. 2. For the dielectron sample, the multi-jet background estimate was obtained directly from the data. The prediction for Drell-Yan production of Z/γ^* is normalized to the observed $Z \rightarrow \ell\ell$ signal. All other MC predictions are normalized to the expected cross sections. Figure 3(a) and (b) show the corresponding cumulative spectra for the $\mu^+\mu^-$ and ee samples. Good agreement is observed between data and the expectation from SM processes over the entire mass region.

Searches for narrow resonances at the Tevatron [6, 8] have placed lower limits in the mass range 600 GeV to 1000 GeV. The region with dilepton masses 120 GeV $< m_{\mu\mu} <$ 200 GeV is part of the region for which resonances have been excluded by the Tevatron, and thus should be dominated by SM processes. The observed good agreement between the data and the prediction in this control region confirms that the SM expectations and the detector performance are well understood.

In the Z peak mass region defined as $60 < m_{\ell\ell} < 120$ GeV, the number of dimuon and dielectron candidates are 16,515 and 8,768 respectively, with very small backgrounds. The expected yields in the control region and high invariant mass regions are listed in Table 1. The agreement between observed the data and expectations is found to be good. It should be noted that the resonance search is shape-based and does not depend on the magnitude of these background predictions.

Table 1: Number of dilepton events with invariant mass in the control region $120 < m < 200$ GeV and the signal region $m > 200$ GeV. The expected number of Z' events in the model shown is given for a region of $\pm 3\sigma$ around the Z' mass. The total background is the sum of the standard model processes listed. Uncertainties include both statistical and systematic components added in quadrature.

Source	number of events			
	Dimuon Sample: $m_{\mu\mu}$		Dielectron Sample: m_{ee}	
	[120 − 200] GeV	> 200 GeV	[120 − 200] GeV	> 200 GeV
CMS data	227	35	109	26
Z'_{SSM} (750 GeV)	—	13.6 ± 2.0	—	8.7 ± 1.3
Total Background	204 ± 28	36.4 ± 4.6	123 ± 16	24.7 ± 3
Z/γ^*	187 ± 28	30.2 ± 4.5	104 ± 16	18.8 ± 2.8
$t\bar{t}$	12.3 ± 2.3	4.2 ± 0.8	7.4 ± 1.8	2.8 ± 0.5
$t\bar{t}$-like events	4.4 ± 0.4	1.7 ± 0.2	2.7 ± 0.6	1.0 ± 0.4
multi-jet events	0.6 ± 0.2	0.2 ± 0.1	8.6 ± 3.4	2.1 ± 0.8

5 Limits on the Production Cross Section

The observed invariant mass spectrum agrees with expectations based on Standard Model processes, therefore limits are set on the possible contributions from a narrow heavy resonance. As

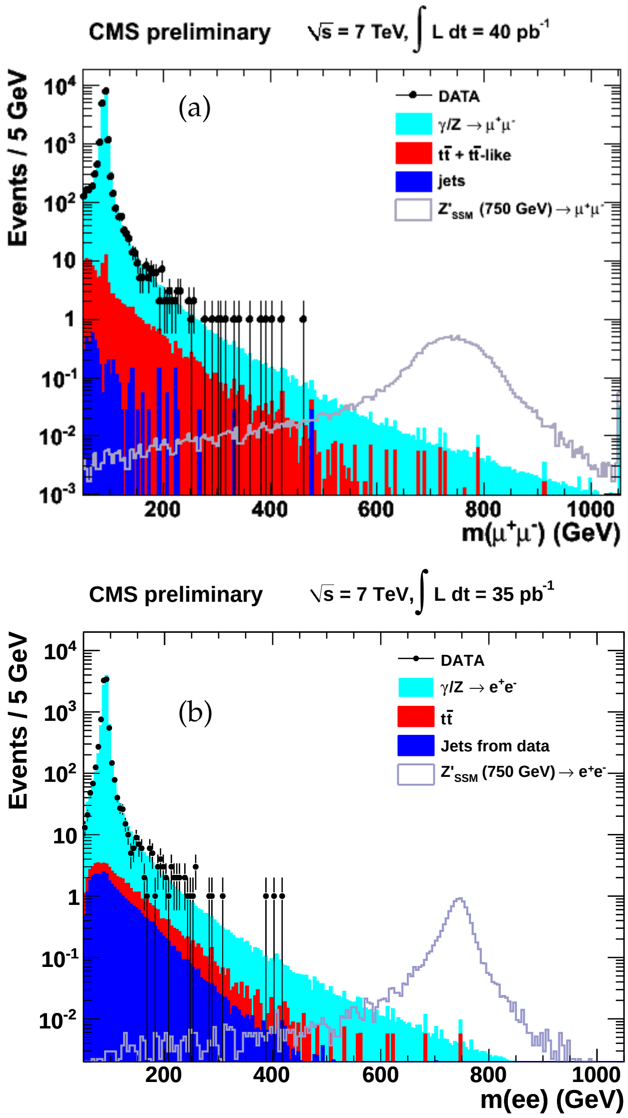

Figure 2: Invariant mass spectrum of (a) $\mu^+\mu^-$ and (b) ee events. The points with error bars represent the CMS data, and the filled histograms represent the expectations from Standard Model processes: Z/γ^*, $t\bar{t}$, $t\bar{t}$-like (tW, diboson production, $Z \to \tau\tau$) and the multi-jet backgrounds. The open histogram shows the signal expected for a Z'_{SSM} with a mass of 750 GeV.

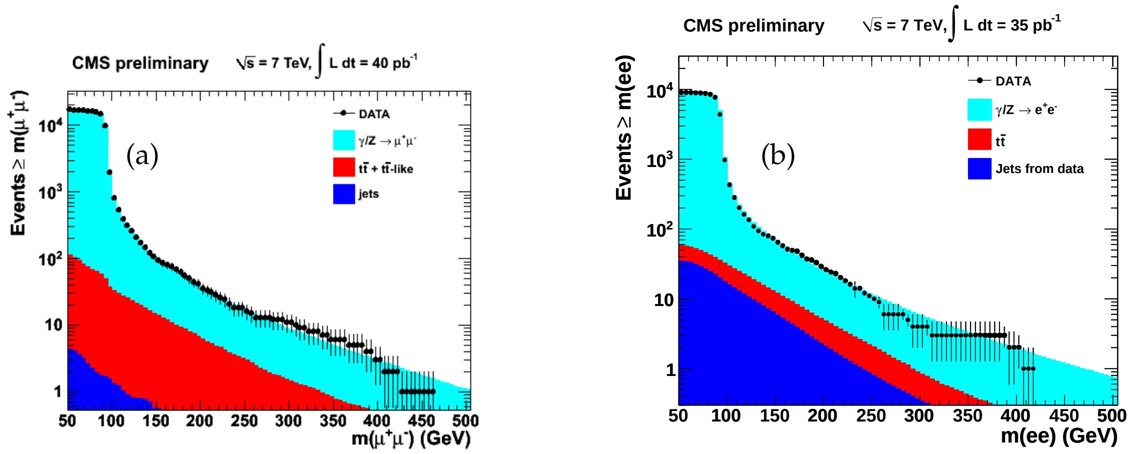

Figure 3: Cumulative invariant mass spectrum of (a) $\mu^+\mu^-$ and (b) ee events. The points with error bars represent the CMS data, and the filled histogram represents the expectations from standard model processes.

noted in the introduction, the parameter of interest is the cross section times branching fraction ratio,

$$R_\sigma = \frac{\sigma(pp \to Z' + X \to \ell\ell + X)}{\sigma(pp \to Z + X \to \ell\ell + X)}. \tag{1}$$

For inferences about R_σ, we first estimate the Poisson mean μ_Z of the number of $Z \to \ell\ell$ events in the sample (i.e., the observed N_Z in the interval, with a small subtraction). The uncertainty on μ_Z is about 1% (almost all statistical) and contributes negligibly to the uncertainty on R_σ.

We then construct an extended unbinned likelihood function for the spectrum of $\ell\ell$ invariant mass values m above 200 GeV, based on a sum of analytic probability density functions (pdfs) for the signal and background shapes.

The pdf $f_\mathrm{S}(m|\Gamma, M, w)$ for the resonance signal is a Breit-Wigner of width Γ and mass M convoluted with a Gaussian resolution function of width w. The width Γ is taken to be that of the Z'_{SSM} (about 3%); as noted below, the high-mass limits are insensitive to this width. The Poisson mean of the yield is $\mu_\mathrm{S} = R_\sigma \cdot \mu_Z \cdot R_\epsilon$, where R_ϵ is the ratio of selection efficiency times detector acceptance for Z' and Z boson decays. μ_B denotes the Poisson mean of the total background yield. A background pdf f_B was chosen and its shape parameters fixed by fitting to the simulated Drell-Yan spectrum in the mass range $200 < m < 2000$ GeV. Two functional forms for f_B were tried with shape parameters α and κ, $f_\mathrm{B}(m|\alpha,\kappa) \sim \exp(-\alpha m^\kappa)$ and $\sim \exp(-\alpha m) m^{-\kappa}$. Both yielded excellent fits for both the dimuon and dielectron spectra, and consistent results; for definiteness we present those obtained with the latter form.

The extended likelihood $\mathcal{L}$ is then

$$\mathcal{L}(\boldsymbol{m}|R_\sigma, M, \Gamma, w, \alpha, \kappa, \mu_\mathrm{B}) = \frac{\mu^N e^{-\mu}}{N!} \prod_{i=1}^{N} \left(\frac{\mu_\mathrm{S}(R_\sigma)}{\mu} f_\mathrm{S}(m_i|M,\Gamma,w) + \frac{\mu_\mathrm{B}}{\mu} f_\mathrm{B}(m_i|\alpha,\kappa) \right), \tag{2}$$

where $\boldsymbol{m}$ denotes the dataset in which the observables are the invariant mass values of the lepton pairs, m_i; N denotes the total number of events observed above 200 GeV; and $\mu = \mu_\mathrm{S} + \mu_\mathrm{B}$ is the Poisson mean from which N is a sample. By focusing on the ratio R_σ, we eliminate the uncertainty (11% at present) in the integrated luminosity, reduce the dependence on experimental acceptance, trigger, and offline efficiencies, and generally obtain a more robust result.

Starting from Eqn. 2, confidence/credible intervals are computed using more than one approach, both frequentist (using likelihood ratios) and Bayesian (multiplying $\mathcal{L}$ by prior pdfs). The upper limits on R_σ are very similar when a uniform prior is used for the signal mean, and we report the Bayesian result (implemented with Markov Chain Monte Carlo in RooStats [25]) for definiteness.

With no candidate events in the region of small expected background above 465 GeV, the result is robust not only with respect to statistical technique, but also with respect to the width of the Z′ and to changes in systematic uncertainties and their functional forms, taken to be log-normal distributions with fractional uncertainties. For R_ϵ, we assign an uncertainty of 8% for the dielectron channel and 3% for the dimuon channel. These values reflect our current understanding of the turn-on at low mass (including PDF uncertainties and mass-dependence of K-factors) as well as the evolution at high mass where cosmic-ray muons exist to study muon performance but not electron performance. The uncertainty in the mass scale affects only the mass region below 500 GeV where there are events, in both channels extrapolating from the well-calibrated observed resonances. For the dielectron channel it is set to 1% based on linearity studies; for the dimuon channel, a sensitivity study showed negligible change of results up to the maximum that might be possible due to alignment effects (several per cent), and was kept fixed at zero in constructing the plots shown.

In the frequentist calculation, the mean background level μ_{B} is the maximum likelihood estimate; in the fully Bayesian calculation a prior must be assigned to the mean background level, but the result is insensitive to reasonable choices (i.e., for which the likelihood dominates the prior).

From the $\mu^+\mu^-$ and ee data, we obtain the upper limits on the cross section ratio R_σ (Eqn. 1) at 95% C.L. shown in Fig. 4(a) and (b), respectively.

In Fig. 4, the predicted cross section ratios for Z'_{SSM} and Z'_ψ production are superimposed together with those for G_{KK} production with dimensionless graviton coupling to SM fields $k/\overline{M_{\mathrm{Pl}}} = 0.05$ and 0.1. The leading order cross section predictions for Z'_{SSM} and Z'_ψ from PYTHIA using CTEQ6.1 PDFs are corrected for a mass dependent K-factor obtained using ZWPRODP [26–29] to account for NNLO contributions. For the RS graviton model, a constant NLO K-factor of 1.6 is used [30]. The uncertainties due to the QCD scale parameter and PDFs are indicated as a band. The NNLO prediction for Z production cross section is 0.97 ± 0.04 nb [21].

After propagating the above-mentioned uncertainties into the comparison of the experimental limits with the predicted cross section ratios, we exclude at 95% C.L. Z' masses M as follows. From the dimuon only analysis, a Z' with standard model-like couplings (Z'_{SSM}) can be excluded below 1027 GeV, the superstring-inspired Z'_ψ below 792 GeV, and RS Kaluza-Klein gravitons G_{KK} below 778 (987) GeV for couplings of 0.05 (0.1) at 95% CL. For the dielectron analysis, at 95% C.L., the production of Z'_{SSM} and Z'_ψ bosons is excluded for masses below 958 and 731 GeV, respectively. The corresponding 95% CL. lower limits on the mass for RS G_{KK} graviton production with couplings of 0.05-0.1 are 729-931 GeV.

5.1 Combined Limits on the Production Cross Section using $\mu^+\mu^-$ and ee events

The above formalism is generalized to combine the results from the $\mu^+\mu^-$ and the ee channels, by defining the combined likelihood as the product of the likelihoods for the individual channels with R_σ forced to be the same value for both channels. The combined limit is shown in Fig. 4 (c).

By combining the $\mu^+\mu^-$ and ee channels, the following 95% C.L. lower limits on the mass of a Z' resonance are obtained: 1140 GeV for the Z'_{SSM}, and 887 GeV for Z'_{ψ} models. RS Kaluza-Klein gravitons are excluded below 855-1079 GeV at 95% C.L. for values of couplings 0.05-0.1. Our observed limits are more restrictive than or comparable to those previously obtained via similar direct searches by the Tevatron experiments [5–8], or indirect searches by LEP-II experiments [9], with the exception for Z'_{SSM}, where the value from LEP-II is most restrictive.

In the narrow-width approximation, the cross section for the process $pp \to Z' + X \to \ell\ell + X$ can be expressed [10, 26] in terms of the quantity $c_u w_u + c_d w_d$, where c_u and c_d contain the information from the model-dependent Z' couplings to fermions in the annihilation of charge 2/3 and charge $-1/3$ quarks, respectively, and where w_u and w_d contain the information about PDFs for the respective annihilation at a given Z′ mass. The translation of the experimental limits into the c_u-c_d plane has been studied in the context of both the narrow-width and finite width approximations. The procedures have been shown to give the same results. In Fig. 5 the limits on the Z' mass are shown as lines in the (c_d, c_u) plane intersected by curves from various models which specify (c_d, c_u) as a function of a model mixing parameter. The point labeled SM corresponds to the Z'_{SSM}; it lies on the more general curve for the generalized sequential standard model (GSM) for which the generators of the $U(1)_{T_{3L}}$ and $U(1)_Q$ gauge groups are mixed with mixing angle α. Then $\alpha = -0.072\pi$ corresponds to the Z'_{SSM} and $\alpha = 0$ and $\pi/2$ define the T_{3L} and Q benchmarks, respectively, which have larger values of (c_d, c_u) and hence larger lower bounds on the masses. Also shown are contours for the E_6 model (with χ, ψ, η, S, and N corresponding to angles 0, 0.5π, -0.29π, 0.13π, and 0.42π, respectively) and Generalized LR models (with R, $B-L$, LR, and Y corresponding to angles 0, 0.5π, -0.13π, and 0.25π, respectively) [26] .

In this plane, the black lines labeled by mass are iso-contours of cross section with constant $c_u + (w_d/w_u)c_d$, where w_d/w_u is in the range 0.5-0.6 for the results relevant here. As this linear combination increases or decreases by an order of magnitude, the mass limits change by roughly 500 GeV.

6 Conclusion

The CMS Collaboration has searched for narrow resonances in the invariant mass spectrum of events with ee and $\mu^+\mu^-$ final states in data corresponding to an integrated luminosity of 35 pb^{-1}and 40 pb^{-1}, respectively. The spectra are consistent with Standard Model expectations and cross section limits were set, normalized to the cross section for Standard Model Z boson production. Mass limits were set on neutral gauge bosons Z' and RS Kaluza-Klein gravitons G_{KK}. A Z' with standard model-like couplings can be excluded below 1140 GeV, the superstring-inspired Z'_{ψ} below 887 GeV, and RS Kaluza-Klein gravitons below 855-1079 GeV for couplings of 0.05-0.1 at 95% C.L.

Acknowledgments

We wish to congratulate our colleagues in the CERN accelerator departments for the excellent performance of the LHC machine. We thank the technical and administrative staff at CERN and other CMS institutes, and acknowledge support from: FMSR (Austria); FNRS and FWO (Belgium); CNPq, CAPES, FAPERJ, and FAPESP (Brazil); MES (Bulgaria); CERN; CAS, MoST, and NSFC (China); COLCIENCIAS (Colombia); MSES (Croatia); RPF (Cyprus); Academy of Sciences and NICPB (Estonia); Academy of Finland, ME, and HIP (Finland); CEA and CNRS/IN2P3 (France); BMBF, DFG, and HGF (Germany); GSRT (Greece); OTKA and NKTH (Hungary);

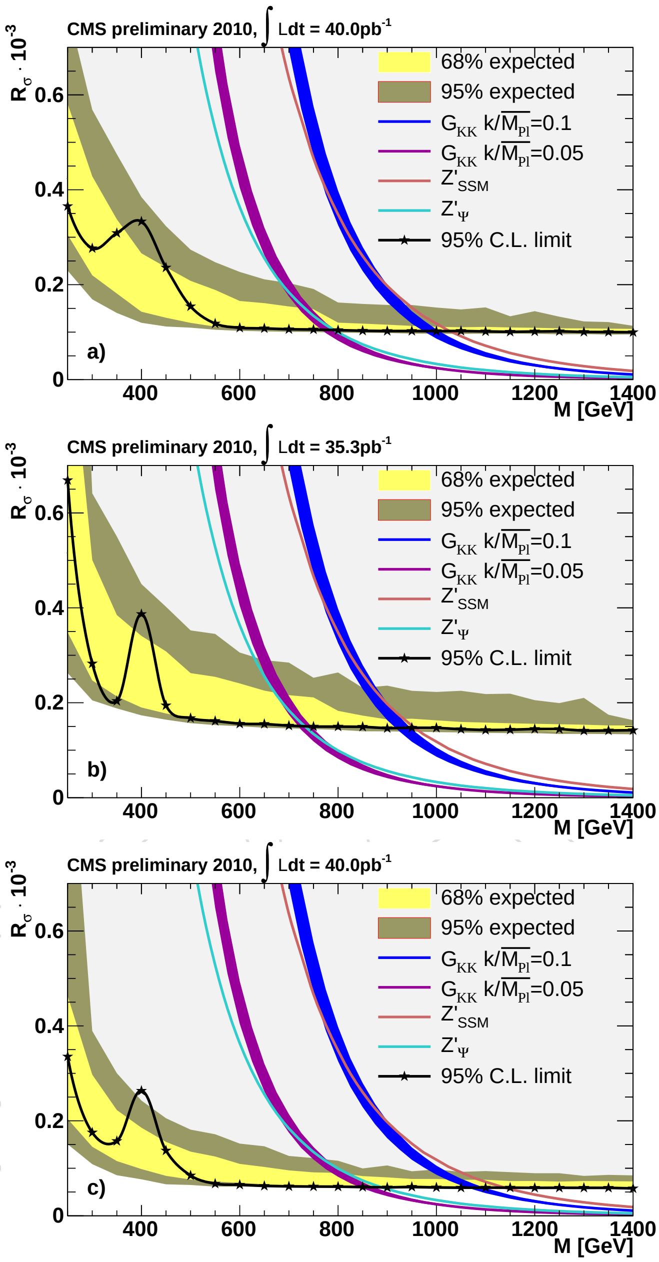

Figure 4: Upper limits on the production ratio of cross section times branching fraction into lepton pairs (R_σ) for Z' and G_{KK}-production and Z boson production. The limits are shown from (a) the $\mu^+\mu^-$ final state, (b) the ee final state and (c) the combined dilepton result. The predicted theoretical cross section ratios along with their uncertainty band are superimposed.

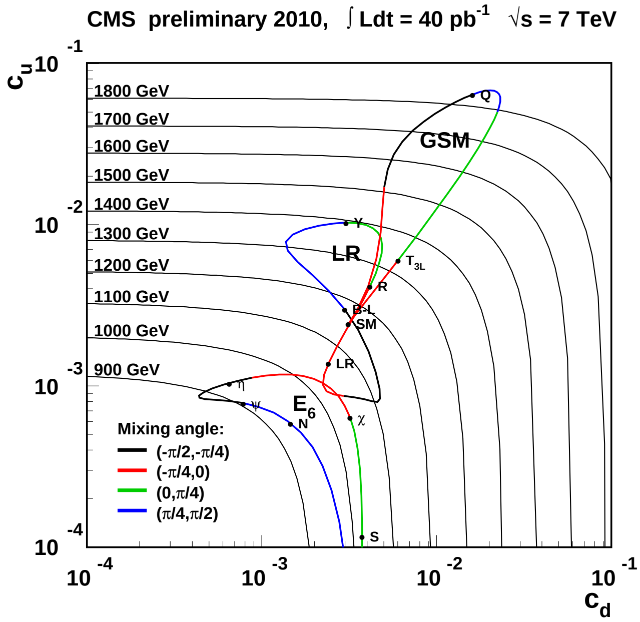

Figure 5: 95% C.L. lower limits on the Z' mass, shown as lines in black in (c_d, c_u) plane in which colored curves for three classes of models are drawn. For any point on a curve, the mass limit corresponding to that (c_d, c_u) is given by the intersected contour. Colors on the curves correspond to different mixing angles of the generators defined in each model.

DAE and DST (India); IPM (Iran); SFI (Ireland); INFN (Italy); NRF and WCU (Korea); LAS (Lithuania); CINVESTAV, CONACYT, SEP, and UASLP-FAI (Mexico); PAEC (Pakistan); SCSR (Poland); FCT (Portugal); JINR (Armenia, Belarus, Georgia, Ukraine, Uzbekistan); MST and MAE (Russia); MSTD (Serbia); MICINN and CPAN (Spain); Swiss Funding Agencies (Switzerland); NSC (Taipei); TUBITAK and TAEK (Turkey); STFC (United Kingdom); DOE and NSF (USA).

References

[1] L. Evans and P. Bryant (editors), “LHC Machine”, *JINST* **3** (2008) S08001. doi:10.1088/1748-0221/3/08/S08001.

[2] A. Leike, “The Phenomenology of extra neutral gauge bosons”, *Phys. Rept.* **317** (1999) 143–250, arXiv:hep-ph/9805494. doi:10.1016/S0370-1573(98)00133-1.

[3] L. Randall and R. Sundrum, “An alternative to compactification”, *Phys. Rev. Lett.* **83** (1999) 4690–4693, arXiv:hep-th/9906064. doi:10.1103/PhysRevLett.83.4690.

[4] L. Randall and R. Sundrum, “A large mass hierarchy from a small extra dimension”, *Phys. Rev. Lett.* **83** (1999) 3370–3373, arXiv:hep-ph/9905221. doi:10.1103/PhysRevLett.83.3370.

[5] D0 Collaboration, “Search for Randall-Sundrum gravitons in the dielectron and diphoton final states with 5.4 fb-1 of data from ppbar collisions at sqrt(s)=1.96 TeV”, *Phys. Rev. Lett.*

104 (2010) 241802, arXiv:1004.1826. doi:10.1103/PhysRevLett.104.241802.

[6] D0 Collaboration, "Search for a heavy neutral gauge boson in the dielectron channel with 5.4 fb^{-1} of $\mathbf{p\bar{p}}$ collisions at $\sqrt{\mathbf{s}} = \mathbf{1.96}$ TeV", *accepted by Phys. Lett. B* (2010) arXiv:1008.2023.

[7] CDF Collaboration, "A search for high-mass resonances decaying to dimuons at CDF", *Phys. Rev. Lett.* **102** (2009) 091805, arXiv:0811.0053. doi:10.1103/PhysRevLett.102.091805.

[8] CDF Collaboration, "Search for High-Mass e^+ e- Resonances in $p\bar{p}$ Collisions at $\sqrt{s}$ = 1.96-TeV", *Phys. Rev. Lett.* **102** (2009) 031801, arXiv:0810.2059. doi:10.1103/PhysRevLett.102.031801.

[9] "LEP electroweak working group, A Combination of preliminary electroweak measurements and constraints on the standard model", arXiv:hep-ex/0612034.

[10] M. S. Carena, A. Daleo, B. A. Dobrescu et al., "Z' gauge bosons at the Tevatron", *Phys. Rev.* **D70** (2004) 093009, arXiv:hep-ph/0408098. doi:10.1103/PhysRevD.70.093009.

[11] CMS Collaboration, "The CMS experiment at the CERN LHC", *JINST* **3** (2008) S08004. doi:10.1088/1748-0221/3/08/S08004.

[12] CMS Collaboration, "Measurements of Inclusive W and Z Cross Sections in pp collisions at $\sqrt{s} = 7$ TeV", *CMS PAS* **EWK-2010-002** (2010).

[13] CMS Collaboration, "Performance of CMS muon identification in pp collisions at $\sqrt{s} = 7$ TeV", *CMS PAS* **MUO-2010-002** (2010).

[14] CMS Collaboration, "Performance of CMS Muon Reconstruction in Cosmic-Ray Events", *JINST* **5** (2010) T03022, arXiv:0911.4994. doi:10.1088/1748-0221/5/03/T03022.

[15] T. Sjostrand, S. Mrenna, and P. Z. Skands, "PYTHIA 6.4 Physics and Manual", *JHEP* **05** (2006) 026, arXiv:hep-ph/0603175.

[16] F. Maltoni and T. Stelzer, "MadEvent: Automatic event generation with MadGraph", *JHEP* **02** (2003) 027, arXiv:hep-ex/0208156.

[17] S. Alioli, P. Nason, C. Oleari et al., "NLO vector-boson production matched with shower in POWHEG", *JHEP* **07** (2008) 060, arXiv:0805.4802. doi:10.1088/1126-6708/2008/07/060.

[18] P. Nason, "A new method for combining NLO QCD with shower Monte Carlo algorithms", *JHEP* **11** (2004) 040, arXiv:hep-ph/0409146. doi:10.1088/1126-6708/2004/11/040.

[19] S. Frixione, P. Nason, and C. Oleari, "Matching NLO QCD computations with Parton Shower simulations: the POWHEG method", *JHEP* **11** (2007) 070, arXiv:0709.2092. doi:10.1088/1126-6708/2007/11/070.

[20] GEANT4 Collaboration, "GEANT4: A simulation toolkit", *Nucl. Instrum. Meth.* **A506** (2003) 250–303. doi:10.1016/S0168-9002(03)01368-8.

[21] K. Melnikov, F. Petriello, Phys. Rev. D74, (2006) 114017.

[22] D. Bourilkov, "Study of parton density function uncertainties with LHAPDF and PYTHIA at LHC", arXiv:hep-ph/0305126.

[23] M. R. Whalley, D. Bourilkov, and R. C. Group, "The Les Houches Accord PDFs (LHAPDF) and Lhaglue", arXiv:hep-ph/0508110.

[24] CMS Collaboration Collaboration, "First Measurement of the Cross Section for Top-Quark Pair Production in Proton-Proton Collisions at $\sqrt{s} = 7$ TeV", *CMS PAS* **TOP-10-001** (2010).

[25] L. Moneta, K. Belasco, K. Cranmer et al., "The RooStats project", arXiv:arXiv:1009.1003v1.

[26] E. Accomando, A. Belyaev, L. Fedeli et al., "Z′ physics with early LHC data", arXiv:arXiv:1010.6058.

[27] R. Hamberg, W. L. van Neerven, and T. Matsuura, "A Complete calculation of the order α_S^2 correction to the Drell-Yan K factor", *Nucl. Phys.* **B359** (1991) 343–405. doi:10.1016/0550-3213(91)90064-5.

[28] W. L. van Neerven and E. B. Zijlstra, "The O(α_S^2) corrected Drell-Yan K-factor in the DIS and $\overline{\mathrm{MS}}$ schemes", *Nucl. Phys.* **B382** (1992) 11–62. doi:10.1016/0550-3213(92)90078-P.

[29] R. Hamberg, T. Matsuura, and W. van Neerven ZWPROD program (1989-2002), http://www.lorentz.leidenuniv.nl/research/neerven/DECEASED/Welcome.html.

[30] P. Mathews, V. Ravindran, and K. Sridhar, "NLO-QCD corrections to dilepton production in the Randall- Sundrum model", *JHEP* **10** (2005) 031, arXiv:hep-ph/0506158. doi:10.1088/1126-6708/2005/10/031.